International Journal of Mechanical Sciences 310 (2026) 111076

Contents lists available at ScienceDirect

International Journal of Mechanical Sciences

journal homepage: www.elsevier.com/locate/ijmecsci

# Characterization of strain-induced anisotropy in isotropic hyperelastic materials via generalized incremental moduli

Emanuele Luigi Carniel [a,b]

[a] Centre for Mechanics of Biological Materials, University of Padova, Italy
[b] Department of Industrial Engineering, University of Padova, Italy

ARTICLE INFO

*Keywords:*
Soft materials
Non-linear elasticity
Hyperelasticity
Generalized incremental moduli
Strain stiffening and softening
Strain induced anisotropy

ABSTRACT

This paper introduces a generalized formulation of incremental elastic moduli for the characterization of strain-induced anisotropy in isotropic hyperelastic materials. The proposed approach extends the classical concept of incremental stiffness moduli, which are traditionally limited to specific deformation modes such as uniaxial stress, simple shear, or hydrostatic stress, by enabling the evaluation of tangent stiffness under arbitrary deformation states. This represents a novel and unified framework for quantifying deformation-induced anisotropy and directional stiffness variations in hyperelasticity.

Detailed mathematical derivations are presented for the computation of generalized incremental moduli, which are applied to both classical and recent isotropic hyperelastic models, including Neo-Hookean, Mooney-Rivlin, Fung-Demiray, and Anssari-Benam formulations. The analytical results reveal how strain-induced anisotropy evolves under different loading conditions, such as uniaxial, equibiaxial, and simple shear, highlighting model-dependent trends in stiffening and softening behavior.

Overall, the study demonstrates that the proposed definition of generalized incremental moduli provides a comprehensive and versatile tool for the analysis of tangent stiffness in hyperelastic materials, with potential applications in material characterization and engineering design.

## 1. Introduction

The framework of linear elasticity constitutes a robust, precisely defined analytical tool, within which model parameters maintain direct physical interpretations and exhibit unambiguous identification via well-established experimental methodologies. Conversely, hyperelasticity is a critical field in the characterization of elastomeric materials and soft biological tissues [1–4], whose application and implementation is mandatory for the development of computational models of soft and biological structures [5–7]. Nevertheless, hyperelasticity remains an actively evolving research area and is characterized by complexities that currently limit extensive engineering applications. As an example, multiple hyperelastic formulations may explain the same experimental results but lead to markedly different predictions when extrapolated beyond the experimental range [8]. At the same time, for any given formulation, a non-optimal experimental design can result in unreliable and/or non-univocal parameters identification [9–11]. The primary challenge of hyperelastic modelling stems from the dependence of mechanical properties on the deformation state, a phenomenon that affects the theoretical formulations and is confirmed by experimental activities [12–14]. Consequently, the constitutive parameters often lose direct physical interpretability and/or applicability in the engineering design, frequently being restricted to representations of mechanical properties in the undeformed configuration [15–18].

Nonetheless, engineering design necessitates accurate knowledge of mechanical properties, such as stiffness moduli, specifically tailored to the intended application and the corresponding deformation regime in which the material operates. Therefore, there arises the necessity to develop rigorous and comprehensive moduli capable of capturing material stiffness under general deformation conditions. Addressing this need, incremental stiffness moduli have been previously introduced [19–22], which describe material properties limited to specific deformational processes, such as uniaxial tension, simple shear, or hydrostatic pressure. Beatty and Stalnaker [19] proposed a definition of the Poisson function for finite elasticity and presented comparisons with experimental data for uni-axial stress conditions. Scott [22] proposed incremental moduli, specifically incremental Young's modulus, incremental Poisson's ratio, and incremental bulk modulus, highlighting their physical significance and calculation based on variations in specific stress-strain states, such as uni-axial and hydrostatic stress. Mihai and

*E-mail address:* emanueleluigi.carniel@unipd.it.

https://doi.org/10.1016/j.ijmecsci.2025.111076
Received 7 August 2025; Received in revised form 15 October 2025; Accepted 26 November 2025
Available online 29 November 2025

Goriely [21] further expanded upon these incremental moduli, explicitly introducing the incremental shear and torsion moduli, and providing comprehensive calculations based on stress-strain derivatives under finite deformation conditions, thus enhancing their physical interpretability and analytical robustness. Recently, Carniel et al [20] developed computational tools for determining incremental moduli and applied them to representative hyperelastic formulations. However, these approaches are mainly restricted to the evaluation of incremental moduli under specific and simplified stress-strain states, which often differ from those occurring in practical material applications. Earlier, Biot [23] introduced stress-dependent incremental moduli, showing that initial stresses can lead to the anisotropization of an otherwise isotropic material. More recently, the concept of generalized elasticity moduli has been advanced, encompassing the characterization of various stiffness attributes (longitudinal, lateral, tangential, and volumetric) pertinent to arbitrary deformation states, thereby constituting a versatile and robust analytical framework [24]. These generalized moduli explicitly account for the directional dependency of material stiffness induced by deformation, a phenomenon recognized as strain-induced anisotropy [25]. The earliest analyses concerning deformation-induced anisotropy date back to the first investigations on the elastic behavior of rubber-like materials. In these studies, an anisotropy factor was introduced to describe the dimensional variations of a material point along the three spatial directions under hydrostatic pressure. This factor allows for the identification of differences in the mechanical response among the different directions when the material point has been subjected to initial stresses [26,27]. Experimental evidence for deformation-induced anisotropy has been widely documented, highlighting its occurrence in elastomers and other materials. Hamed and Song [28] reported significant anisotropy arising in uncrosslinked elastomers subjected to large deformation, while Toki et al [29] demonstrated through synchrotron X-ray diffraction that molecular orientation induced by uniaxial deformation significantly alters the mechanical response of vulcanized polyisoprene rubbers. Horgan et al [30], Diani et al [31], Dargazany and Itskov [32], Machado et al [33], Marckmann et al [34], and Anssari-Benam et al [35] investigated the effects of strain and related damage mechanisms, such as the Mullins effect, on the development of anisotropy in rubber-like materials. Mahnken and Dammann [25] analyzed the anisotropization of polymeric materials caused by the alignment of macromolecular chains along the principal tensile loading directions, and developed a constitutive framework to evaluate their induced anisotropic behavior. Further studies by Vader et al [36] using collagen gels and Ustinov [37] on various elastomers reinforced these findings, showing clear directional dependencies in mechanical properties following deformation. Mokhireva et al. [38] analyzed strain-induced anisotropy in elastomeric nanocomposites, showing that deformation promotes progressive filler alignment and, consequently, directional stiffening. Xian et al [39] highlighted strain-induced anisotropy in filled elastomers, explicitly incorporating strain-induced crystallization and the deformation-driven alignment of macromolecular chains. Mahjoubi et al [40] examined strain-induced phase transformation in semicrystalline polylactide, emphasizing how the resulting microstructural rearrangements lead to variations in mechanical properties and progressive anisotropization. Gajo and Bigoni [41], Gajo [42], Cudny and Staszewska [43] and Cudny et al [44] conducted investigations, within a hyperelasticity framework, into stress-induced anisotropy of various soils and sands, and presented comparisons between theoretical predictions and experimental data. The mentioned previous studies have proposed mathematical frameworks and reported experimental observations of strain-induced anisotropy, but they have not provided practical instruments for its quantitative characterization and control. By expressing stiffness as a function of deformation magnitude and orientation, the generalized elasticity moduli proposed by Carniel [24] allow for a systematic quantification of strain-induced stiffening, softening, and anisotropy. Accordingly, this paper provides a theoretical framework and practical applications illustrating the evolution of such phenomena in isotropic hyperelastic materials. The Materials and Methods section reports the fundamentals of hyperelasticity theory together with the definition of generalized incremental moduli, as well as their computation for specific constitutive models. Specifically, the Neo-Hookean model [16] offers a simplified, polynomial-based approach commonly employed for moderate strain applications. The Mooney-Rivlin formulation [15,45] incorporates both first and second invariants of strain, providing increased flexibility and improved accuracy in representing complex deformation behaviors. The Fung-Demiray model [46–48] uses an exponential formulation, effectively capturing pronounced stiffening behaviors characteristic of elastomers and biological tissues at higher strains [49]. Finally, the recent formulation proposed by Anssari-Benam [50] integrates molecular-kinetic theory parameters, aiming for comprehensive modelling of rubber-like materials, linking theoretical predictions more closely to experimental observations. Furthermore, the proposed methodology is also applied to the case of isotropic linear elasticity, demonstrating that the downgraded form of the theory correctly recovers the classical relationships reported in the literature. The computation and graphical representation of the generalized incremental moduli, presented in the Results section, reveal for different deformation states, such as uniaxial and equibiaxial tension and compression, and simple shear, the evolution of the mechanical properties with respect to the loading directions, thereby illustrating the progressive stiffening/softening and anisotropization of the material, as extensively addressed in the Discussion section.

## 2. Materials and methods

The analysis of anisotropization processes occurring in a hyperelastic material as a consequence of deformation is carried out by employing the concept of generalized incremental moduli. In this regard, Section 2.1 provides, after a brief review of the fundamentals of hyperelasticity theory, the definition of the generalized incremental moduli and the description of the procedures for their computation. Subsequently, Section 2.2 addresses application cases concerning the calculation of the generalized incremental moduli for some typical isotropic hyperelastic formulations. Finally, in order to establish a connection with a well-known framework, Section 2.3 applies the proposed approach to the classical theory of isotropic linear elasticity.

### 2.1. Generalized incremental moduli

For an isotropic hyperelastic material point, the stress-strain behavior is defined through an isotropic hyperelastic potential $W$. The second Piola-Kirchhoff stress tensor $\mathbf{S} \in Sym$ is related to the right Cauchy-Green deformation tensor $\mathbf{C} = \mathbf{F}^T\mathbf{F} \in Psym$, being $\mathbf{F} \in Lin^+$ the deformation gradient, via the derivative of the strain energy function, as $\mathbf{S} = 2\partial W/\partial \mathbf{C}$. The strain energy $W$ is frequently expressed as a function of the principal invariants $I_1 = tr(\mathbf{C})$, $I_2 = (1/2)\left[{I_1}^2 - tr\left(\mathbf{C}^2\right)\right]$ and $J = \det(\mathbf{F}) = \sqrt{\det(\mathbf{C})}$ [51,52]. By applying the chain rule and considering that $\partial I_1/\partial \mathbf{C} = \mathbf{1}$, $\partial I_2/\partial \mathbf{C} = I_1\mathbf{1} - \mathbf{C}$ and $\partial J/\partial \mathbf{C} = (1/2)J\mathbf{C}^{-1}$, it follows [53]:

$$\mathbf{S} = JW_J\mathbf{C}^{-1} + 2W_1\mathbf{1} + 2W_2(I_1\mathbf{1} - \mathbf{C}), \tag{1}$$

where $W_1$, $W_2$ and $W_J$ are the derivatives of $W$ with respect to $I_1$, $I_2$ and $J$, respectively. To evaluate the actual stress state of the material, the Cauchy stress tensor $\boldsymbol{\sigma} \in Sym$ can be obtained through the push-forward operation:

$$\boldsymbol{\sigma} = \frac{1}{J}\mathbf{F}\mathbf{S}\mathbf{F}^T = W_J\mathbf{1} + \frac{2}{J}W_1\mathbf{B} + \frac{2}{J}W_2\left(I_1\mathbf{B} - \mathbf{B}^2\right), \tag{2}$$

where $\mathbf{B} = \mathbf{F}\mathbf{F}^T \in Psym$ is the left Cauchy-Green strain tensor.

The mechanical response of the material point can be characterized

by generalized incremental stiffness moduli. Given an orthonormal reference system $\mathbf{n}, \mathbf{p}, \mathbf{q}$, for a generic strain state $\mathbf{B}$, the generalized incremental Young's moduli and Poisson's ratios are defined by considering a uni-axial stress variation along direction $\mathbf{n}$, such as $d\sigma_{nn}$ (Fig. 1), and evaluating the corresponding stretch variations along the directions $\mathbf{n}$, $\mathbf{p}$ and $\mathbf{q}$ of stretch components $\lambda_{nn}$, $\lambda_{pp}$ and $\lambda_{qq}$, such as $d\lambda_{nn}$, $d\lambda_{pp}$ and $d\lambda_{qq}$.

The generalized incremental Young's modulus $E_n = \lambda_{nn}(d\sigma_{nn}/d\lambda_{nn})$ along direction $\mathbf{n}$ is defined as [24]:

$$\begin{aligned} E_n = {}& 2{\lambda_{nn}}^2 \frac{\partial \sigma}{\partial \mathbf{B}} :: (\mathbf{n}\otimes\mathbf{n}\otimes\mathbf{n}\otimes\mathbf{n}) - \\ & -2\nu_{np}{\lambda_{pp}}^2 \frac{\partial \sigma}{\partial \mathbf{B}} :: (\mathbf{n}\otimes\mathbf{n}\otimes\mathbf{p}\otimes\mathbf{p}) - \\ & -2\nu_{nq}{\lambda_{qq}}^2 \frac{\partial \sigma}{\partial \mathbf{B}} :: (\mathbf{n}\otimes\mathbf{n}\otimes\mathbf{q}\otimes\mathbf{q}) \end{aligned} \tag{3}$$

Analogously, the generalized incremental Poisson's ratios $\nu_{np} = -(\lambda_{nn}/\lambda_{pp})(d\lambda_{pp}/d\lambda_{nn})$ and $\nu_{nq} = -(\lambda_{nn}/\lambda_{qq})(d\lambda_{qq}/d\lambda_{nn})$ describing transverse strain along orthogonal directions $\mathbf{p}$ and $\mathbf{q}$ are computed as:

$$\nu_{np} = -\frac{{\lambda_{nn}}^2}{{\lambda_{pp}}^2} \frac{\left[\frac{\partial\sigma}{\partial\mathbf{B}} :: (\mathbf{p}\otimes\mathbf{p}\otimes\mathbf{q}\otimes\mathbf{q})\right]\left[\frac{\partial\sigma}{\partial\mathbf{B}} :: (\mathbf{q}\otimes\mathbf{q}\otimes\mathbf{n}\otimes\mathbf{n})\right] - \left[\frac{\partial\sigma}{\partial\mathbf{B}} :: (\mathbf{q}\otimes\mathbf{q}\otimes\mathbf{q}\otimes\mathbf{q})\right]\left[\frac{\partial\sigma}{\partial\mathbf{B}} :: (\mathbf{p}\otimes\mathbf{p}\otimes\mathbf{n}\otimes\mathbf{n})\right]}{\left[\frac{\partial\sigma}{\partial\mathbf{B}} :: (\mathbf{p}\otimes\mathbf{p}\otimes\mathbf{p}\otimes\mathbf{p})\right]\left[\frac{\partial\sigma}{\partial\mathbf{B}} :: (\mathbf{q}\otimes\mathbf{q}\otimes\mathbf{q}\otimes\mathbf{q})\right] - \left[\frac{\partial\sigma}{\partial\mathbf{B}} :: (\mathbf{p}\otimes\mathbf{p}\otimes\mathbf{q}\otimes\mathbf{q})\right]\left[\frac{\partial\sigma}{\partial\mathbf{B}} :: (\mathbf{q}\otimes\mathbf{q}\otimes\mathbf{p}\otimes\mathbf{p})\right]}, \tag{4}$$

$$\nu_{nq} = -\frac{{\lambda_{nn}}^2}{{\lambda_{qq}}^2} \frac{\left[\frac{\partial\sigma}{\partial\mathbf{B}} :: (\mathbf{q}\otimes\mathbf{q}\otimes\mathbf{p}\otimes\mathbf{p})\right]\left[\frac{\partial\sigma}{\partial\mathbf{B}} :: (\mathbf{p}\otimes\mathbf{p}\otimes\mathbf{n}\otimes\mathbf{n})\right] - \left[\frac{\partial\sigma}{\partial\mathbf{B}} :: (\mathbf{p}\otimes\mathbf{p}\otimes\mathbf{p}\otimes\mathbf{p})\right]\left[\frac{\partial\sigma}{\partial\mathbf{B}} :: (\mathbf{q}\otimes\mathbf{q}\otimes\mathbf{n}\otimes\mathbf{n})\right]}{\left[\frac{\partial\sigma}{\partial\mathbf{B}} :: (\mathbf{p}\otimes\mathbf{p}\otimes\mathbf{p}\otimes\mathbf{p})\right]\left[\frac{\partial\sigma}{\partial\mathbf{B}} :: (\mathbf{q}\otimes\mathbf{q}\otimes\mathbf{q}\otimes\mathbf{q})\right] - \left[\frac{\partial\sigma}{\partial\mathbf{B}} :: (\mathbf{p}\otimes\mathbf{p}\otimes\mathbf{q}\otimes\mathbf{q})\right]\left[\frac{\partial\sigma}{\partial\mathbf{B}} :: (\mathbf{q}\otimes\mathbf{q}\otimes\mathbf{p}\otimes\mathbf{p})\right]}, \tag{5}$$

where ${\lambda_{nn}}^2 = \mathbf{n}\cdot\mathbf{B}\cdot\mathbf{n}$, ${\lambda_{pp}}^2 = \mathbf{p}\cdot\mathbf{B}\cdot\mathbf{p}$ and ${\lambda_{qq}}^2 = \mathbf{q}\cdot\mathbf{B}\cdot\mathbf{q}$, while '$\cdot$' and '$::$' denote the single (i.e., if $\mathbf{B}$ is a second rank tensor and $\mathbf{n}$ a vector, vector $\mathbf{v} = \mathbf{B}\cdot\mathbf{n}$ has components $v_i = B_{ij}n_j$) and quadruple (i.e., if $\mathbb{C}$ and $\mathbb{N}$ are fourth rank tensor, operation $\mathbb{C} :: \mathbb{N}$ leads to the scalar quantity $\mathbb{C}_{ijkl}\mathbb{N}_{ijkl}$) contractions, respectively, while '$\otimes$' is the dyadic operator (i.e., if $\mathbf{a}$ and $\mathbf{b}$ are vectors, $\mathbf{a}\otimes\mathbf{b}$ is a second rank tensor with components $a_ib_j$; while if $\mathbf{A}$ and $\mathbf{B}$ are second rank tensors, $\mathbf{A}\otimes\mathbf{B}$ is a fourth rank tensor with components $A_{ij}B_{kl}$) [54–56].

By assuming a hydrostatic pressure variation $d\sigma_p$ and measuring the corresponding volumetric variation $dJ$, it is also possible to define a generalized incremental bulk modulus $K_v = (J/3)d\sigma_p/dJ$, where $\sigma_p = tr(\boldsymbol{\sigma})/3$, aimed at evaluating the evolution of compressibility under a generic stress-strain condition [24]:

$$K_v = \frac{2}{9} tr\left(\frac{\partial\boldsymbol{\sigma}}{\partial\mathbf{B}} : \mathbf{B}\right). \tag{6}$$

The fourth rank stiffness tensor $\partial\boldsymbol{\sigma}/\partial\mathbf{B}$ [57,58] can be computed starting from Eq. (2) and by applying the chain rule:

$$\begin{aligned} \frac{\partial\sigma}{\partial\mathbf{B}} = {}& \frac{\partial W_J}{\partial\mathbf{B}}\otimes\mathbf{1} + \frac{2}{J}\frac{\partial W_1}{\partial\mathbf{B}}\otimes\mathbf{B} + \\ & + \frac{2}{J}\frac{\partial W_2}{\partial\mathbf{B}}\otimes(I_1\mathbf{B}-\mathbf{B}^2) - \frac{1}{J}(W_1 + I_1W_2)\mathbf{B}^{-1}\otimes\mathbf{B} + \\ & + \frac{1}{J}W_2(\mathbf{B}^{-1}\otimes\mathbf{B}^2 - 2\mathbf{B}\otimes\mathbf{1}) + \frac{2}{J}(W_1 + I_1W_2)\mathbf{I} \end{aligned} \tag{7}$$

being $\partial W_1/\partial\mathbf{B} = (1/2)JW_{1J}\mathbf{B}^{-1} + W_{11}\mathbf{1} + W_{12}(I_1\mathbf{B} - \mathbf{B}^2)$, $\partial W_2/\partial\mathbf{B} = (1/2)JW_{2J}\mathbf{B}^{-1} + W_{21}\mathbf{1} + W_{22}(I_1\mathbf{B} - \mathbf{B}^2)$ and $\partial W_J/\partial\mathbf{B} = (1/2)JW_{JJ}\mathbf{B}^{-1} + W_{J1}\mathbf{1} + W_{J2}(I_1\mathbf{B} - \mathbf{B}^2)$, where $W_{11} = \partial^2W/\partial{I_1}^2$, $W_{22} = \partial^2W/\partial{I_2}^2$, $W_{JJ} = \partial^2W/\partial J^2$, $W_{12} = W_{21} = \partial^2W/\partial I_1\partial I_2$, $W_{1J} = W_{J1} = \partial^2W/\partial I_1\partial J$ and $W_{2J} = W_{J2} = \partial^2W/\partial I_2\partial J$ are the second derivatives of $W$ with respect to the principal invariants, while $\mathbf{I}$ is the fourth rank unit tensor. In the unstrained configuration (i.e., $\mathbf{B} = \mathbf{1}$), the stiffness tensor assumes the following isotropic conformation:

$$\begin{aligned} \left.\frac{\partial\sigma}{\partial\mathbf{B}}\right|_{\mathbf{B}=\mathbf{1}} = {}& \left(\frac{1}{2}W_{JJ} + 2W_{1J} + 4W_{2J} + 2W_{11} + \right. \\ & \left. + 8W_{12} + 8W_{22} - W_1 - 4W_2\right)\mathbf{1}\otimes\mathbf{1} + \\ & + 2(W_1 + 3W_2)\mathbf{I} \end{aligned} \tag{8}$$

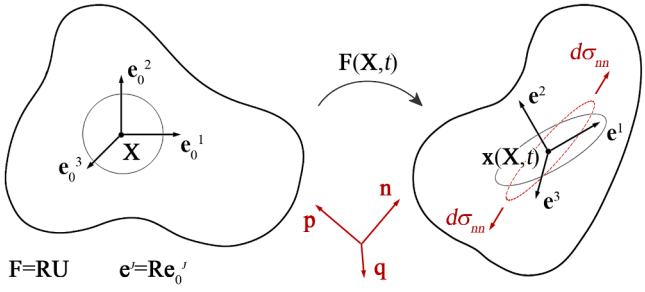


**Fig. 1.** Material point kinematics and mechanics. The deformation gradient $\mathbf{F} = \mathbf{RU}$ describes the deformation of a material point through the stretch tensor $\mathbf{U} = \sqrt{\mathbf{C}} \in Psym$, and its rigid-body rotation through the rotation tensor $\mathbf{R} \in Orth^+$. The latter allows the transformation from the lagrangian reference system $\mathbf{e}_0{}^j$ to the eulerian reference system $\mathbf{e}^j$. Given an orthonormal reference system defined by the directions $\mathbf{n}$, $\mathbf{p}$ and $\mathbf{q}$, it is possible to consider a uniaxial variation of stress along direction $\mathbf{n}$. By measuring the resulting stretch variations along directions $\mathbf{n}$, $\mathbf{p}$ and $\mathbf{q}$, the generalized incremental Young's moduli and Poisson's ratios can be defined.

The isotropy of the stiffness tensor implies that, in the unstrained configuration, the generalized incremental Young's modulus and Poisson's ratios are independent of direction. However, when evaluated in a strained configuration, the directionality of the strain tensor **B** induces a corresponding directionality in the stiffness tensor. As a result, the generalized moduli exhibit directional dependence, thereby revealing an anisotropic mechanical response. This phenomenon, referred to as strain-induced anisotropy, has been experimentally observed even in materials that are initially isotropic.

### 2.2. Isotropic hyperelastic formulations

In order to concretely analyze the trend of generalized incremental moduli, representative isotropic hyperelastic formulations based on strain invariants were considered. The dependence of the strain energy function $W$ on the strain is commonly expressed by decoupling the volumetric and the isovolumetric contributions [59,60], $U$ and $\widetilde{W}$ respectively:

$$W(\mathbf{C}) = U(J) + \widetilde{W}(\widetilde{I}_1, \widetilde{I}_2), \tag{9}$$

where $\widetilde{I}_1 = J^{-2/3} I_1$ and $\widetilde{I}_2 = J^{-4/3} I_2$ are the first and second isovolumetric invariants. The following expression of the volumetric term is frequently assumed [61]:

$$U(J) = \frac{K}{2}(J-1)^2, \tag{10}$$

where $K$ specifies the bulk modulus in the reference configuration. The Neo-Hookean model adopts a polynomial form of the strain energy function, as follows [16]:

$$\widetilde{W}^{NH}(\widetilde{I}_1) = C_1(\widetilde{I}_1 - 3), \tag{11}$$

where $C_1 = G/2$, being $G$ the shear modulus in the reference configuration.

The Mooney-Rivlin strain energy involves both the first and the second invariants in a polynomial formulation [15,45]:

$$\widetilde{W}^{MR}(\widetilde{I}_1, \widetilde{I}_2) = C_1(\widetilde{I}_1 - 3) + C_2(\widetilde{I}_2 - 3), \tag{12}$$

where $C_1 + C_2 = G/2$.

Otherwise, exponential formulation of the strain energy, such as in the Fung-Demiray model, can be assumed [46–48]:

$$\widetilde{W}^{FD}(\widetilde{I}_1) = \frac{C_1}{\alpha_1}\{\exp[\alpha_1(\widetilde{I}_1 - 3)] - 1\}, \tag{13}$$

where $C_1 = G/2$, while $\alpha_1$ quantifies strain stiffening phenomena.

Recently, more general formulations have been reported, such as the one proposed by Anssari-Benam [62]:

$$\widetilde{W}^{AB}(\widetilde{I}_1) = \frac{3(n-1)}{2n}\mu N\left[\frac{\widetilde{I}_1 - 3}{3N(n-1)} - \ln\left(\frac{\widetilde{I}_1 - 3N}{3 - 3N}\right)\right], \tag{14}$$

where $\mu = nG(1-N)/(1-nN)$, while $n$ and $N$ are parameters from the kinetic molecular theory [50,62–64].

Details of first and second derivatives of the strain energy functions are reported in Appendix A.

### 2.3. Isotropic linear elasticity

To assess the validity of the proposed theoretical framework, its application to the case of isotropic linear elasticity is here considered. In this context, the corresponding expressions for the Young's modulus, Poisson's ratio, and bulk modulus are derived and compared with their well-established classical counterparts.

The strain energy density is therefore defined according to the St. Venant-Kirchhoff formulation [65–67]:

$$W^{EL}(\mathbf{E}) = \frac{1}{2}\kappa[tr(\mathbf{E})]^2 + \mu tr(\mathbf{E}^2), \tag{15}$$

where $\kappa$ and $\mu$ denote the Lamé constants, and $\mathbf{E} = (1/2)(\mathbf{C} - \mathbf{1})$ is the Green-Lagrange strain tensor [51]. Standard computations lead to the Cauchy stress tensor:

$$\boldsymbol{\sigma} = \frac{1}{J}\left[\frac{\kappa}{2}(I_1 - 3)\mathbf{B} + \mu(\mathbf{B}^2 - \mathbf{B})\right]. \tag{16}$$

Consequently, the derivative of the Cauchy stress tensor with respect to **B** can be evaluated as:

$$\begin{aligned}\frac{\partial \boldsymbol{\sigma}}{\partial \mathbf{B}} = \frac{1}{J}\Big\{&\frac{\kappa}{2}[\mathbf{1}\otimes\mathbf{B} + (I_1 - 3)\mathbf{I}] + \mu(\mathbf{B}\otimes\mathbf{1} + \mathbf{1}\otimes\mathbf{B} - \mathbf{I}) \\ &- \frac{1}{2}\left[\frac{\kappa}{2}(I_1 - 3)\mathbf{B} + \mu(\mathbf{B}^2 - \mathbf{B})\right]\otimes\mathbf{B}^{-1}\Big\}.\end{aligned} \tag{17}$$

Invoking infinitesimal strains and working in the undeformed configuration [68,69], which is consistent with linear elasticity, the above relation becomes:

$$\frac{\partial \boldsymbol{\sigma}}{\partial \mathbf{B}} = \frac{\kappa}{2}\mathbf{1}\otimes\mathbf{1} + 2\mu\mathbf{I}. \tag{18}$$

Since $\mathbf{1}\otimes\mathbf{1}$ and $\mathbf{I}$ are strain-independent and isotropic fourth rank tensors [56], the resulting tensor $\partial\boldsymbol{\sigma}/\partial\mathbf{B}$ exhibits no dependence on the deformation state and thus remains isotropic. No specific loading condition or orientation needs to be prescribed for the computation of the incremental Young's modulus reported in Eq. (3), which results in $E_n = \mu(3\kappa + 2\mu)/(\kappa + \mu)$, the incremental Poisson's ratio reported in Eq. (4), which results in $\nu_{np} = \kappa/2(\kappa + \mu)$, and the incremental bulk modulus reported in Eq. (6), which results in $K_v = \kappa + (2/3)\mu$. The derived expressions are found to be fully consistent with the classical relationships among the constitutive parameters of isotropic linear elasticity [22,70].

## 3. Results

The previous calculations were applied to evaluate the trend of generalized incremental moduli for the proposed isotropic hyperelastic formulations. First, Section 3.1 considers the uniaxial stress state, analyzing the evolution of the incremental Young's modulus, the incremental Poisson's ratio and the incremental bulk modulus with deformation, under both tensile and compressive conditions. Subsequently, more complex stress-strain states are examined, namely equibiaxial tension and compression (Section 3.2) and simple shear (Section 3.3), for which representative plots are presented to illustrate the behavior of the incremental Young's modulus.

### 3.1. Uniaxial loading

To provide a clear and immediate overview, generalized incremental moduli were computed under uniaxial tensile and compressive conditions along direction $\mathbf{e}^3$. Values of longitudinal stretch $\lambda_{33}$ ranging between 0.4 and 2 were assumed. Transversal stretches $\lambda_{11} = \lambda_{22}$ were computed by solving the nonlinear equation derived from the boundary condition of null lateral stress $\sigma_{11} = \sigma_{22} = 0$ [49]. Fig. 2 presents the results for the different hyperelastic formulations. With regard to the Neo-Hookean model, graphs show the trends of the incremental Young's modulus (Fig. 2a), the incremental Poisson's ratios (Fig. 2b), the incremental bulk modulus (Fig. 2c) and the anisotropy ratio (Fig. 2c), the latter being defined as the ratio between the incremental Young's modulus along the loading direction and that along a lateral direction. Constitutive parameters $K = 4.667$MPa and $C_1 = 0.5$MPa were assumed, which entail a $\nu^0 = 0.4$ Poisson's ratio in the undeformed configuration. Keeping fixed the initial Poisson ratio $\nu^0$ and modifying parameters $D$ and $G = 2C_1$ did not influence the trend of the anisotropy

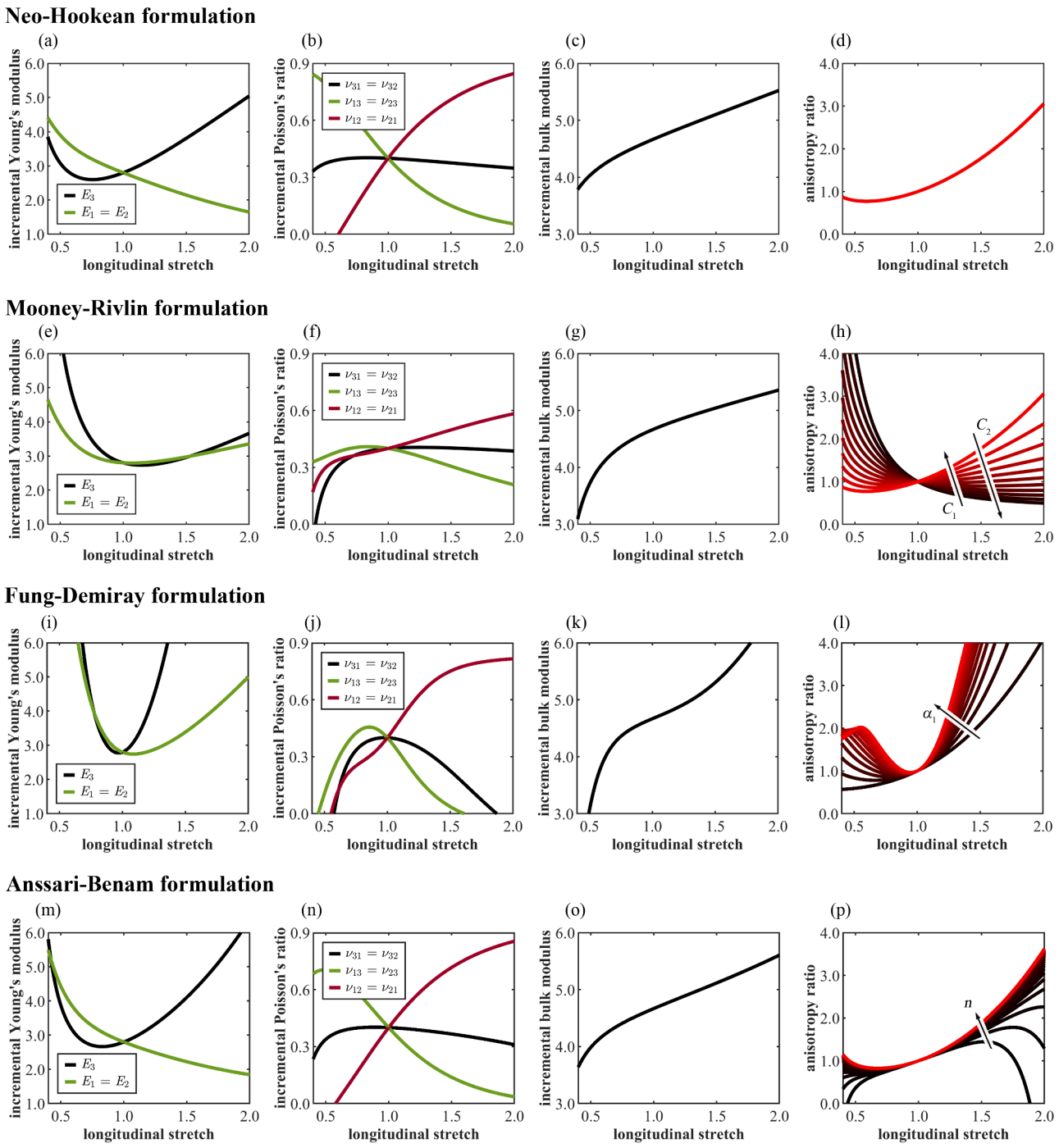


**Fig. 2.** Analysis of generalized incremental moduli for uniaxial tensile and compressive loading along direction $\mathbf{e}^3$. Results are reported for the Neo-Hookean formulation ($K = 4.667$MPa and $C_1 = 0.5$MPa) (a-d), the Mooney-Rivlin formulation ($K = 4.667$MPa and $C_1 = C_2 = 0.25$MPa) (e-h), the Fung-Demiray formulation ($K = 4.667$MPa, $C_1 = 0.5$MPa and $\alpha_1 = 1$) (i-l), and the Anssari-Benam formulation ($K = 4.667$MPa, $\mu = 0.8571$MPa, $n = 2$ and $N = 4$) (m-p). Trend of incremental Young's moduli $E_3$ (black curve) and $E_1 = E_2$ (green curve) with stretch (a,e,i,m). Trend of incremental Poisson's ratios $\nu_{31} = \nu_{32}$ (black curve), $\nu_{13} = \nu_{23}$ (green curve), and $\nu_{12} = \nu_{21}$ (red curve) with stretch (b) (b,f,j,n). Trend of the incremental bulk modulus with stretch (c,g,k,o). Evolution of the anisotropy ratio $E_3/E_1 = E_3/E_2$ with stretch: Neo-Hookean formulation (d); Mooney-Rivlin formulation with parameter $C_1$ and $C_2$ ranging between 0 MPa and 0.5 MPa (initial Poisson ratio and shear stiffness were kept constant) (h); Fung-Demiray formulation with values of parameter $\alpha_1$ ranging between 0 and 3 (initial Poisson ratio and shear stiffness were kept constant) (l); Anssari-Benam formulation with values of parameter $n$ ranging between 0.5 and 7 (initial Poisson ratio and shear stiffness were kept constant) (p).

ratio. Similarly, Figs. 2e to 2p report the results for the other hyperelastic formulations. With reference to the Mooney-Rivlin model (Figs. 2e-h), constitutive parameters $K = 4.667$MPa and $C_1 = C_2 = 0.25$MPa were assumed. Keeping fixed the Poisson's ratio in the undeformed configuration $\nu^0 = 0.4$ and the initial shear stiffness $G = 2(C_1 + C_2) = 1$MPa, values of parameters $C_1$ and $C_2$ were modified to evaluate the influence on the anisotropy ratio (Fig. 2h). For the Fung-Demiray model (Fig. 2i-l) constitutive parameters $K = 4.667$MPa, $C_1 = 0.5$MPa and $\alpha_1 = 1$ were assumed. The anisotropy ratio was evaluated for $\alpha_1$ ranging between 0 and 3, keeping fixed the initial Poisson's ratio $\nu^0 =$

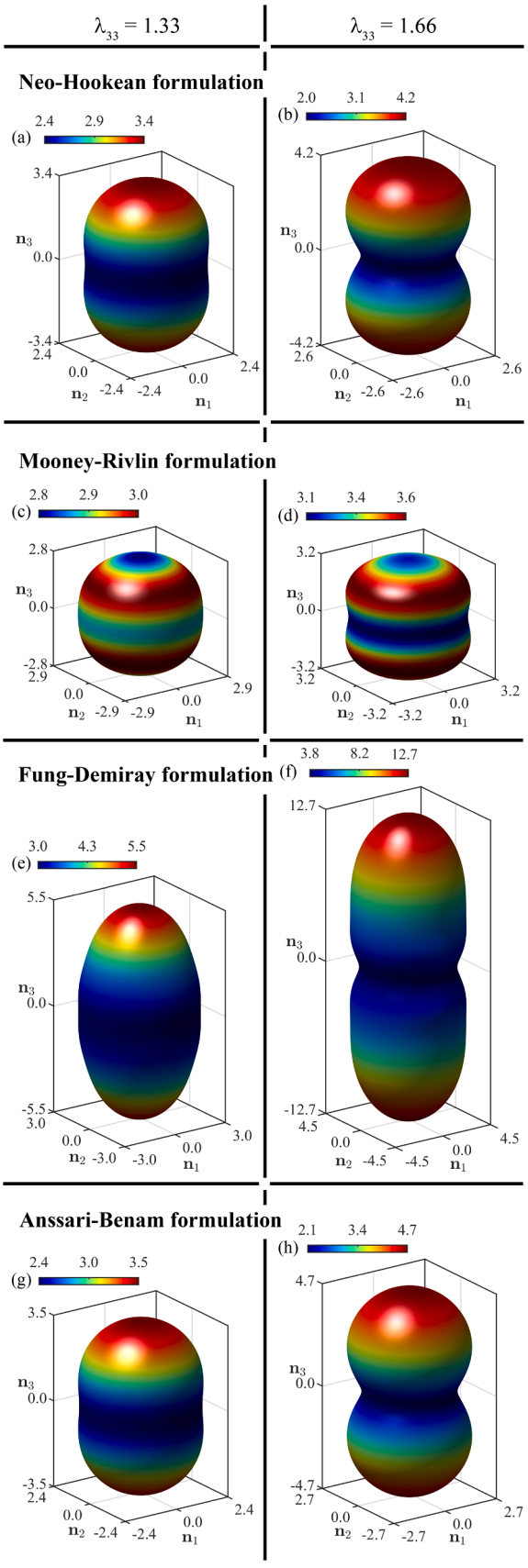


*(caption on next column)*

**Fig. 3.** Analysis of generalized incremental Young's modulus for uniaxial tensile loading along direction $\mathbf{e}^3$. Results are reported for the Neo-Hookean formulation ($K = 4.667$MPa and $C_1 = 0.5$MPa) (a,b), the Mooney-Rivlin formulation ($K = 4.667$MPa and $C_1 = C_2 = 0.25$MPa) (c,d), the Fung-Demiray formulation ($K = 4.667$MPa, $C_1 = 0.5$MPa and $\alpha_1 = 1$) (e,f), and the Anssari-Benam formulation ($K = 4.667$MPa, $\mu = 0.8571$MPa, $n = 2$ and $N = 4$) (g,h). Polar envelops of the generalized Young's modulus $E_n$ along a generic direction $\mathbf{n}$ are reported for uniaxial tensile loading corresponding to $\lambda_{33} = 1.33$ (a,c,e,g) and $\lambda_{33} = 1.66$ (b,d,f,h).

0.4 and the initial shear stiffness $G = 2C_1 = 1$MPa (Fig. 2l). Finally, with reference to the Anssari-Benam formulation (Fig. 2m-p), constitutive parameters $K = 4.667$MPa, $\mu = 0.8571$MPa, $n = 2$ and $N = 4$ were assumed. Keeping fixed the Poisson's ratio in the undeformed configuration $\nu^0 = 0.4$ and the initial shear stiffness $G = \mu(1 - nN)/[n(1 - N)] = 1$MPa, parameter $n$ was modified to evaluate the influence on the anisotropy ratio (Fig. 2p). The constitutive parameters were selected without reference to a specific material, assuming stiffness characteristics typical of elastomeric materials and ensuring the comparability of results among the different hyperelastic formulations.

The anisotropic polar envelopes of the incremental Young's modulus in different deformed configurations are reported in Figs. 3 and 4 for Neo-Hookean (Figs. 3a,b and 4a,b), Mooney-Rivlin (Figs. 3c,d and 4c,d), Fung-Demiray (Figs. 3e,f and 4e,f) and Anssari-Benam (Figs. 3g,h and 4g,h) formulations. Plots are provided considering two uniaxial tensile conditions, such as $\lambda_{33} = 1.33$ (Figs. 3a,c,e,g) and $\lambda_{33} = 1.66$ (Figs. 3b,d,f,h), and two uniaxial compressive conditions, such as $\lambda_{33} = 0.80$ (Figs. 4a,c,e,g) and $\lambda_{33} = 0.60$ (Figs. 4b,d,f,h).

### 3.2. Equibiaxial loading

Aiming to further investigate the trend of generalized incremental moduli, they have been computed under equibiaxial tensile and compressive conditions in the plane generated by directions $\mathbf{e}^1$ and $\mathbf{e}^2$. Values of applied stretches $\lambda_{11}$ and $\lambda_{22}$ ranging between 0.80 and 1.66 were assumed. Transversal stretch $\lambda_{33}$ was computed by solving the nonlinear equation derived from the boundary condition of null lateral stress $\sigma_{33} = 0$ [16]. Fig. 5 provides an overview of the envelopes of the generalized Young's modulus for the investigated hyperelastic formulations, considering both tensile ($\lambda_{11} = \lambda_{22} = 1.66$) and compressive ($\lambda_{11} = \lambda_{22} = 0.80$) conditions.

### 3.3. Simple shear

Finally, the trend of generalized Young's modulus was investigated for simple shear in the plane generated by directions $\mathbf{e}^1$ and $\mathbf{e}^3$. The following expression was assumed for the left Cauchy-Green strain tensor:

$$\mathbf{B} = \begin{bmatrix} 1+\gamma^2 & 0 & \gamma \\ 0 & 1 & 0 \\ \gamma & 0 & 1 \end{bmatrix}, \tag{19}$$

where $\gamma$ is the shear strain [71,72]. The polar envelopes of the generalized Young's modulus are reported in Fig. 6 for the different hyperelastic formulations, together with cartesian plots depicting the trend of generalized Young's modulus in the $\mathbf{e}^1$ - $\mathbf{e}^3$ plane for $\gamma = 0.80$.

For the purpose of performing a comparison among the different hyperelastic formulations and assessing the influence of selected constitutive parameters, the envelopes of the generalized Young's modulus were constructed under a simple shear condition ($\gamma = 0.8$) for various parameter sets (Fig. 7), such as $C_1$ and $C_2$ for the Mooney-Rivlin formulation (parameter $K = 4.667$MPa was kept constant) (Figs. 7a-d), $\alpha_1$ for the Fung-Demiray model (parameters $K = 4.667$MPa and $C_1 = 0.5$MPa were kept constant) (Figs. 7a-d) (Figs. 7e-h), $n$ and $N$ for the Anssari-Benam formulation (parameter $K = 4.667$MPa was kept

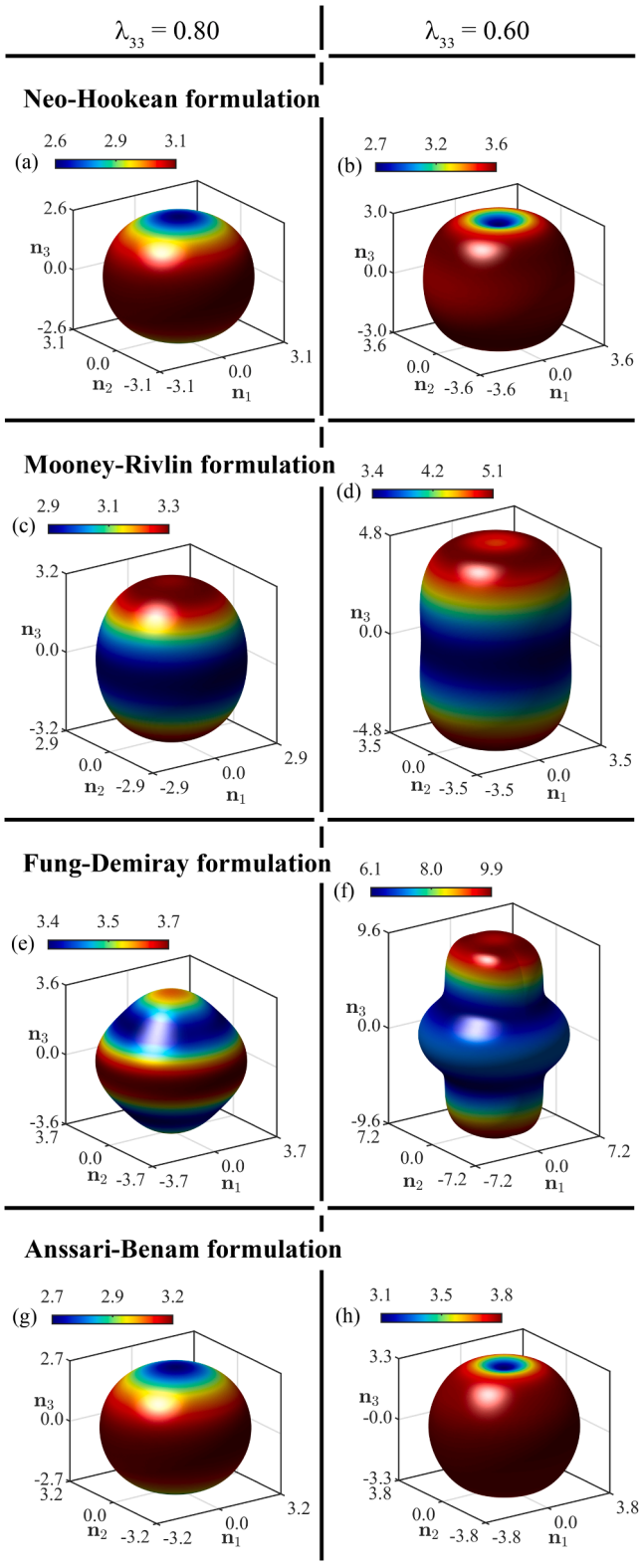


**Fig. 4.** Analysis of generalized incremental Young's modulus for uniaxial compressive loading along direction $\mathbf{e}^3$. Results are reported for the Neo-Hookean formulation ($K = 4.667$MPa and $C_1 = 0.5$MPa) (a,b), the Mooney-Rivlin formulation ($K = 4.667$MPa and $C_1 = C_2 = 0.25$MPa) (c,d), the Fung-Demiray formulation ($K = 4.667$MPa, $C_1 = 0.5$MPa and $\alpha_1 = 1$) (e,f), and the Anssari-Benam formulation ($K = 4.667$MPa, $\mu = 0.8571$MPa, $n = 2$ and $N = 4$) (g,h). Polar envelops of the generalized Young's modulus $E_n$ along a generic direction $\mathbf{n}$ are reported for uniaxial compressive loading corresponding to $\lambda_{33} = 0.8$ (a,c,e,g) and $\lambda_{33} = 0.6$ (b,d,f,h).

constant, while parameter $\mu = nG(1-N)/(1-nN)$ was adjusted to ensure $G = 1$MPa) (Figs. 7i-l). The choice of a simple shear configuration was motivated by its ability to simultaneously generate tensile and compressive principal stress components [73], thus providing a comprehensive representation of material response. In all cases, the constitutive parameters were selected with the aim of highlighting the predictive capabilities and distinctive features of each formulation, rather than reproducing the behavior of a specific material.

## 4. Discussion

The present paper reports the computation and the representation of the generalized incremental moduli for several isotropic hyperelastic formulations, considering different types of stress-strain conditions. With regard to uniaxial loading along direction $\mathbf{e}^3$, the analysis of the trends of incremental moduli with strain (Fig. 2) and the polar envelopes (Figs. 3,4) clearly highlights the process of anisotropization due to the strong loading directionality. The $\mathbf{e}^1$ - $\mathbf{e}^2$ plane remains a plane of isotropy, consistent with the equivalence of these directions under the applied loading, resulting in a transversely isotropic configuration. Under uniaxial tension, all the analyzed hyperelastic formulations show a significant increase in the longitudinal modulus $E_3$ (Figs. 2a,e,i,m), which corresponds to an elongation of the generalized Young's modulus envelope (Fig. 3). The Mooney-Rivlin model (Fig. 2e) shows an exception, with an initial slight decrease in $E_3$ followed by an increasing trend, depending on the assumed constitutive parameters. The lateral moduli $E_1$ and $E_2$ tend to decrease in the Neo-Hookean (Fig. 2a) and Anssari-Benam formulations (Fig. 2m), while they increase in the Mooney-Rivlin (Fig. 2e) and Fung-Demiray models (Fig. 2i), with the latter showing an initial slight drop followed by a marked increase. The mechanical response observed is consistent with the microstructural evolution undergone, for instance, by elastomeric materials during progressive elongation along a specific direction. In the undeformed configuration, an elastomeric material exhibits a random coil arrangement of entangled macromolecular chains [74–76]. The application of uniaxial loading leads to the gradual disentanglement and alignment of these macromolecules along the loading direction. This microstructural reorganization, leading to deformation-induced anisotropy, has been well documented both theoretically [25,77,78] and experimentally [28,29]. For uniaxial compression, all models predict an overall growth of the longitudinal modulus $E_3$ (Figs. 2a,e,i,m), except for an initial drop at small strains (Figs. 2a,i,m). The lateral moduli $E_1$ and $E_2$ generally increase. It is worth noting, as also confirmed by the envelopes of the generalized Young's modulus, that the Neo-Hookean (Figs. 2a, 3a,b, 4a, b), Fung-Demiray (Figs. 2i, 3e,f, 4e,f), and Anssari-Benam (Figs. 2m, 3g, h, 4g,h) formulations exhibit greater stiffening along the loading direction under tension, whereas under compression the stiffening becomes more pronounced in the orthogonal plane. In contrast, the Mooney–Rivlin formulation, for the assumed set of constitutive parameters, exhibits the opposite trend (Figs. 2e, 3c,d, 4c,d).

For the generalized Poisson's ratios (Figs. 2b,f,j,n), the diagrams start from the common isotropic undeformed state and then diverge toward trends compatible with transversely isotropic behavior [79–81]. As an example, the trends of the generalized Poisson's ratios for the Neo-Hookean (Fig. 2b) and the Anssari-Benam (Fig. 2n) formulations can be examined under uniaxial tension along direction $\mathbf{e}^3$. A marked increase in stiffness is observed along direction $\mathbf{e}^3$, accompanied by a reduction along directions $\mathbf{e}^1$ and $\mathbf{e}^2$ (Figs. 2a,m). Correspondingly, significant variations occur in the Poisson's ratios $\nu_{13}$ and $\nu_{12}$. The Poisson's ratio $\nu_{13}$ decreases with increasing deformation, as the progressive anisotropy leads to enhanced stiffness along direction $\mathbf{e}^3$. In fact, when the material is loaded along direction $\mathbf{e}^1$, this stiffness limits the lateral deformation along direction $\mathbf{e}^3$. At the same time, to maintain continuity in compressibility, the reduced contraction along direction $\mathbf{e}^3$ is compensated by a greater contraction along direction $\mathbf{e}^2$, resulting in

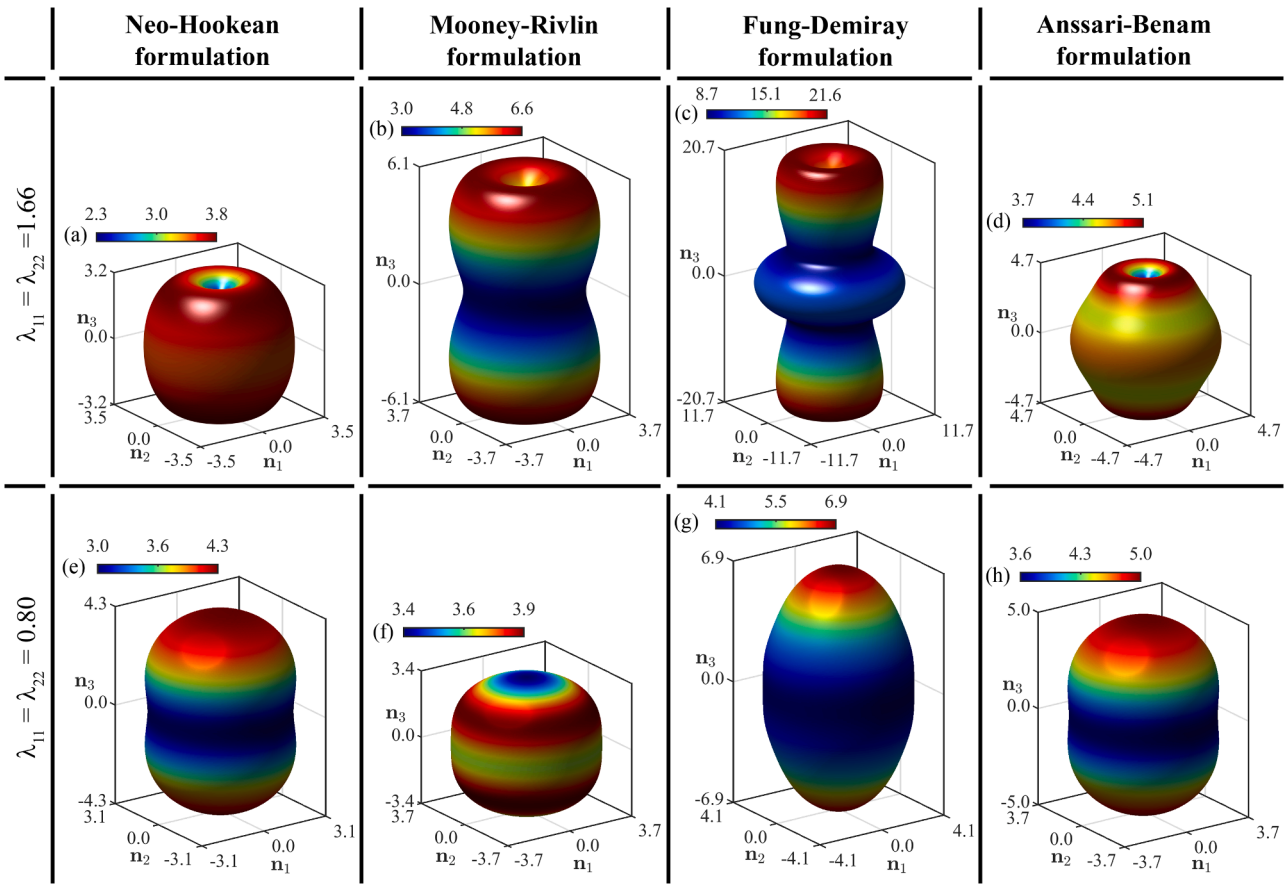


**Fig. 5.** Polar envelopes of generalized incremental Young's modulus $E_n$ along a generic direction $\mathbf{n}$ for equibiaxial tensile ($\lambda_{11} = \lambda_{22} = 1.66$) (a-d) and compressive ($\lambda_{11} = \lambda_{22} = 0.80$) (e-h) loading conditions. Envelopes are reported for the Neo-Hookean formulation ($K = 4.667$MPa and $C_1 = 0.5$MPa) (a,e), the Mooney-Rivlin formulation ($K = 4.667$MPa and $C_1 = C_2 = 0.25$MPa) (b,f), the Fung-Demiray formulation ($K = 4.667$MPa, $C_1 = 0.5$MPa and $\alpha_1 = 0.5$MPa) (c,g) and the Anssari-Benam formulation ($K = 4.667$MPa, $\mu = 0.8571$MPa, $n = 2$ and $N = 4$) (d,h).

an increase in $\nu_{12}$. Under uniaxial compression along direction $\mathbf{e}^3$, the increase in stiffness is more pronounced along directions $\mathbf{e}^1$ and $\mathbf{e}^2$. This produces the opposite trend for the Poisson ratios, with $\nu_{13}$ increasing and $\nu_{12}$ decreasing as the deformation along direction $\mathbf{e}^3$ progresses. Regarding the Poisson's ratios $\nu_{31}$ and $\nu_{32}$, in uniaxial loading along direction $\mathbf{e}^3$, directions $\mathbf{e}^1$ and $\mathbf{e}^2$ define a plane of isotropy, with homogeneous stiffness variations that do not generate lateral deformation imbalance. Overall, variations in the Poisson's ratios are directly related to changes in the deviatoric and volumetric stiffness components (Figs. 2c,g,k,o), which can be evaluated as reported by Carniel [24].

The different evolution of longitudinal modulus $E_3$ compared to lateral moduli $E_1$ and $E_2$ illustrates the anisotropy process, further quantified by the anisotropy ratio diagrams (Figs. 2d,h,l,p). All formulations show significant anisotropization under tensile loading, while under compression the degree of anisotropy is model-dependent, being more pronounced in the Mooney-Rivlin and Fung-Demiray formulations with specific parameters combinations. In this sense, the anisotropy ratio diagrams provide a means to evaluate the influence of selected constitutive parameters, such as the stiffness distribution between $C_1$ and $C_2$ for the Mooney-Rivlin formulation, the parameter $\alpha_1$ for the Fung-Demiray model, and the parameter $n$ for the Anssari-Benam formulation, on the model behavior.

With reference to a uniaxial tension condition, the envelopes of the generalized Young's modulus exhibit, for all formulations, a clear tendency toward anisotropization (Fig. 3). With regard to compressive uniaxial loading, for the Neo-Hookean (Figs. 4a,b) and Anssari-Benam (Figs. 4g,h) models, the generalized Young's modulus envelope shows only slight deviations from spherical isotropic symmetry under compression. In contrast, the Mooney-Rivlin (Figs. 4c,d) and Fung-Demiray models (Figs. 4e,f) display more complex patterns, indicating stronger anisotropization.

For equibiaxial loading in the $\mathbf{e}^1$ - $\mathbf{e}^2$ plane (Fig. 5), a transition from isotropic to transversely isotropic symmetry is observed, being $\mathbf{e}^1$ - $\mathbf{e}^2$ the isotropic plane again. The Neo-Hookean (Figs. 5a,b) and Anssari-Benam (Figs. 5g,h) models show minor deviations from spherical shape of the polar envelop, while the Mooney-Rivlin (Figs. 5c,d) and Fung-Demiray (Figs. 5e,f) formulations exhibit marked deviations, particularly under tension (Figs. 6c,e), confirming their greater susceptibility to anisotropy.

Finally, the analysis of simple shear behavior confirms the development of anisotropy with deformation (Fig. 6). In simple shear in the $\mathbf{e}^1$ - $\mathbf{e}^3$ plane, two quadrants, the first and third, experience predominant tension, while the second and fourth are mainly in compression. In the Neo-Hookean (Figs. 6a,e) and Anssari-Benam (Figs. 6d,h) models, there is a marked increase in stiffness in the tensile quadrants, with a less evident effect in compression quadrants. For the Mooney-Rivlin (Figs. 6b,f) and Fung-Demiray (Figs. 6c,g) formulations, the response is more complex, showing greater stiffening in compression for the former and greater stiffening in tension for the latter. With reference again to the simple shear condition, the influence of specific constitutive parameters on the morphology of the envelope of the generalized Young's modulus was analyzed for the hyperelastic formulations (Fig. 7). For the Mooney-Rivlin model, a progressive redistribution of stiffness from parameter $C_1$ to parameter $C_2$ was analyzed (Figs. 7a-d). Starting from a condition equivalent to the Neo-Hookean model (i.e., $C_2 = 0$), a gradual migration of stiffness was observed from directions

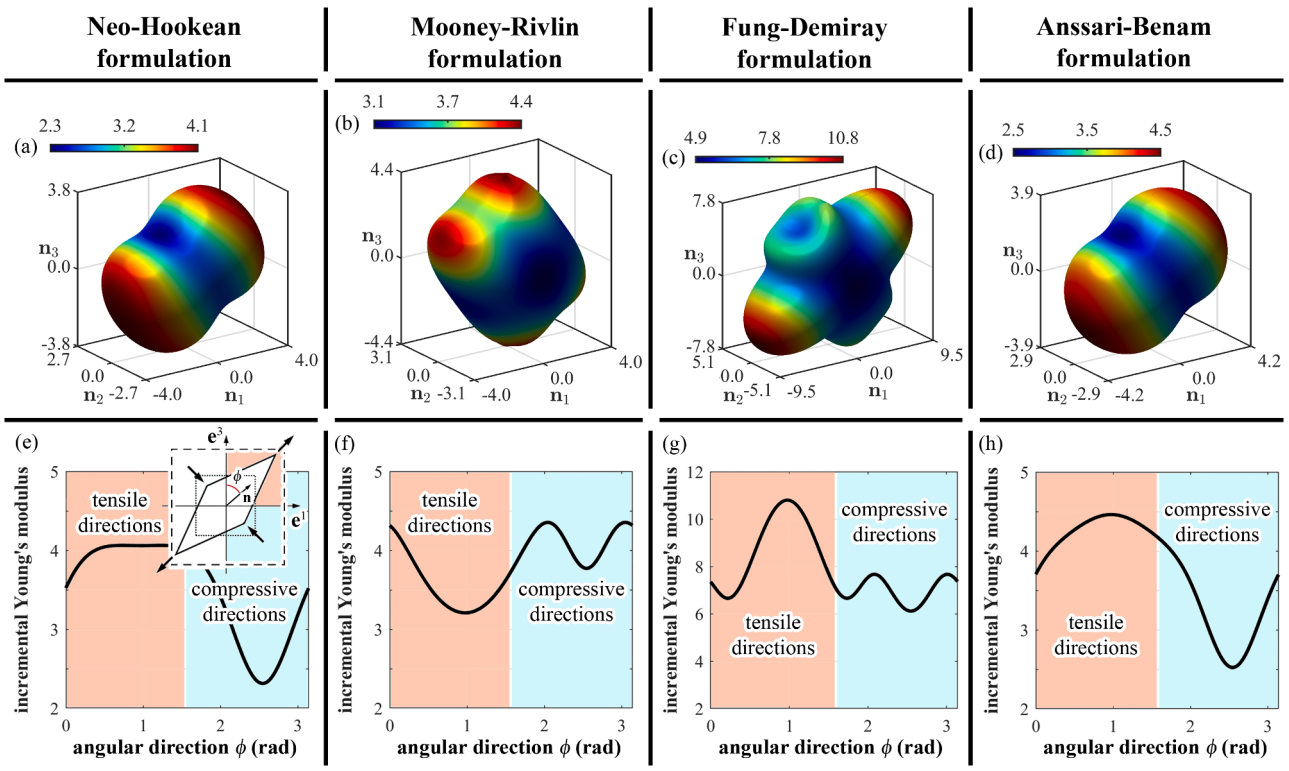


**Fig. 6.** Trend of generalized incremental Young's modulus for simple shear with $\gamma = 0.8$. Fully three-dimensional envelopes of generalized modulus $E_n$ along a generic direction $\mathbf{n}$ (a-d) are reported together with cartesian plots (e-h) depicting the trend of the generalized Young's modulus in the $\mathbf{e}^1$ - $\mathbf{e}^3$ plane. Results are reported for the Neo-Hookean formulation ($K = 4.667$MPa and $C_1 = 0.5$MPa) (a,e), the Mooney-Rivlin formulation ($K = 4.667$MPa and $C_1 = C_2 = 0.25$MPa) (b,f), the Fung-Demiray formulation ($K = 4.667$MPa, $C_1 = 0.5$MPa and $\alpha_1 = 0.5$MPa) (c,g) and the Anssari-Benam formulation ($K = 4.667$MPa, $\mu = 0.8571$MPa, $n = 2$ and $N = 4$) (d,h).

pertaining to the quadrants subjected to tension toward those subjected to compression. In the case of the Fung-Demiray formulation, the effect of the nonlinearity parameter $\alpha_1$ was examined (Figs. 7e-h). For $\alpha_1 = 0$, the response moves toward that of the Neo-Hookean model, whereas increasing values of $\alpha_1$ result in a progressively more pronounced anisotropization of the mechanical response. Finally, for the Anssari-Benam formulation, a distinct tendency toward anisotropy is observed for decreasing values of the parameters $n$ and $N$, indicating a stronger directional dependence of stiffness under shear deformation (Figs. 7i-l).

From the analyses presented above, it emerges that all the investigated hyperelastic formulations exhibit deformation-induced anisotropy, although with different magnitudes and directional characteristics. This phenomenon is particularly pronounced in the Fung-Demiray and the Anssari-Benam models, as observed from the polar envelopes, where the parameter $\alpha_1$ and parameters $n$ and $N$ play a major role in influencing the anisotropization process. It should also be noted that, in the case of the Mooney-Rivlin model, the redistribution of stiffness between $C_1$ and $C_2$ leads to different tendencies toward anisotropization: under tension, the effect is more pronounced when $C_1$ predominates, whereas under compression it becomes more evident when $C_2$ is dominant.

## 5. Conclusions

The analyses presented in this study demonstrate the effectiveness of the generalized incremental moduli in characterizing strain-induced phenomena, such as stiffening, softening, and anisotropization, in isotropic hyperelastic materials. Applied to both classical and contemporary formulations (Neo-Hookean, Mooney-Rivlin, Fung-Demiray, and Anssari-Benam), this framework provides a unified and rigorous description of the evolution of mechanical properties under various deformation states, including uniaxial and equibiaxial tension, compression, and simple shear. The results reveal a progressive departure from isotropy, with distinct stiffness variations along the principal loading directions. The generalized incremental moduli thus represent a quantitative tool for assessing such directional effects and for elucidating the mechanisms underlying deformation-induced anisotropy. Beyond the theoretical contribution, the proposed approach offers practical relevance for evaluating the tangent stiffness of hyperelastic materials under specific loading conditions and in engineering design. In this sense, the generalized incremental moduli may serve as a conceptual bridge between constitutive modeling and the design of soft or rubber-like components, where local stiffness adaptation under large deformations is crucial, such as in elastomeric device optimization, soft robotics, biomechanics, and in silico medicine [82–86].

Limitations of the present work must be acknowledged. This study focused on isotropic materials in their undeformed configuration, neglecting pre-existing anisotropy or microstructural heterogeneity that may be present in real materials. Moreover, the results are based on theoretical and analytical computations, without experimental validation under complex deformation states. Future research should therefore include systematic experimental investigations to verify and calibrate the theoretical predictions, as well as possible extensions of the framework to inherently anisotropic or fiber-reinforced materials. As an example, future experimental activities should combine standard material testing machines with ultrasound devices, to enable the measurement of elastic moduli as a function of the applied strain and their directional dependence, as it has been already proposed by Sasaki et al [87]. Such developments would further strengthen the applicability and reliability of the generalized incremental moduli concept as a comprehensive tool for both material characterization and engineering design.

Finally, it must be underlined that the present work deals with a definition of incremental moduli exclusively within the framework of the theory of elasticity. However, materials that are traditionally

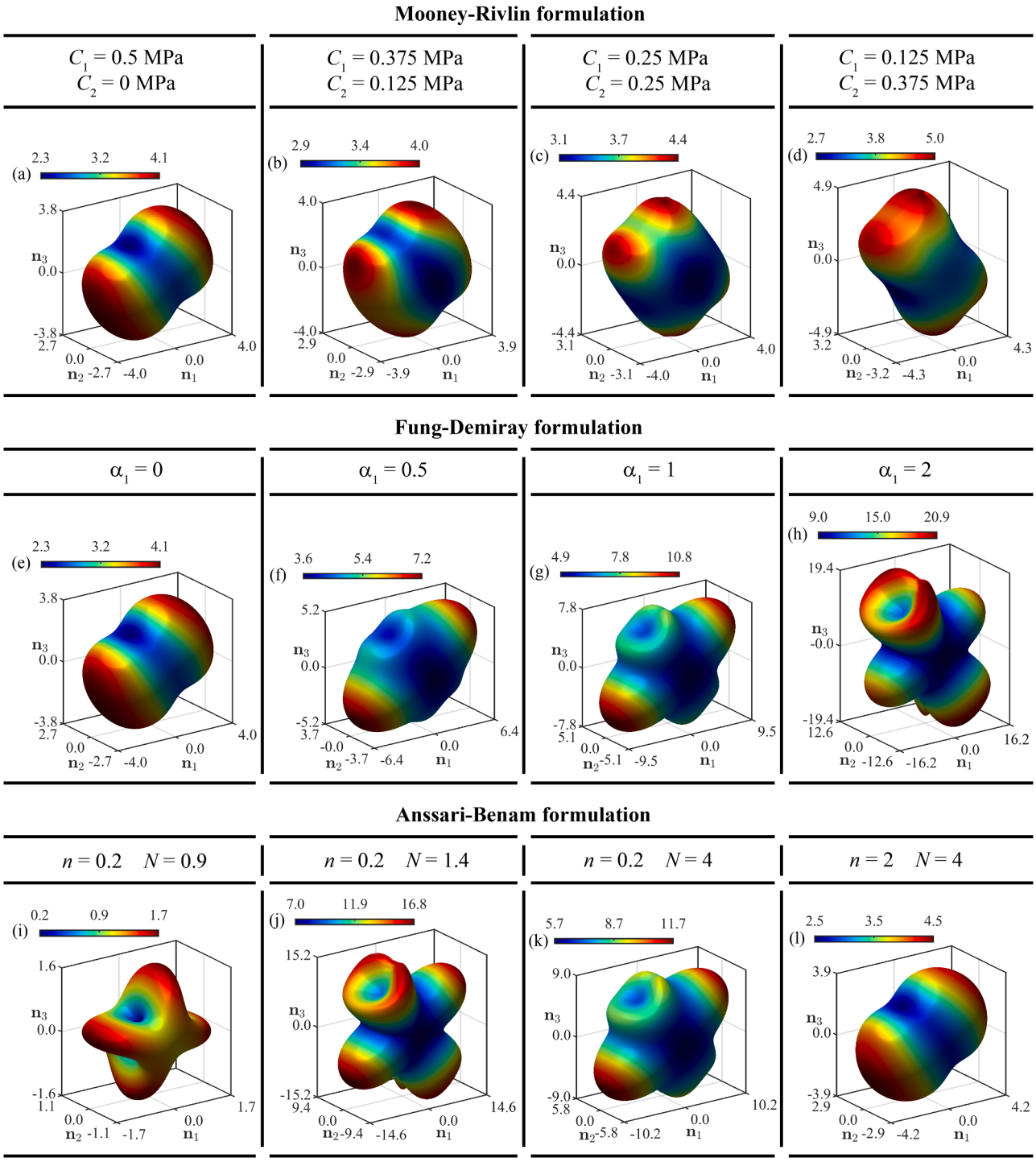


**Fig. 7.** Trend of the generalized incremental Young's modulus under simple shear conditions with $\gamma = 0.8$. Polar envelopes of generalized modulus $E_n$ along a generic direction $\mathbf{n}$ are reported for the Mooney-Rivlin formulation, assuming a progressive transfer of stiffness from $C_1$ to $C_2$ (a-d); for the Fung-Demiray formulation, assuming increasing values of the nonlinearity parameter $\alpha_1$ (e-h); and for the Anssari-Benam formulation, assuming combinations corresponding to increasing values of the parameters $n$ and $N$ (i-l).

modeled as hyperelastic, such as elastomers and soft biological tissues, typically exhibit a time-dependent mechanical response. In such cases, the hyperelastic core of a viscoelastic formulation serves to describe either the instantaneous response and the thermodynamic equilibrium behavior [88,89]. Ongoing research activities are directed toward developing a formal definition of incremental moduli that can represent the time evolution of mechanical properties, taking as a reference the concepts of creep modulus, relaxation modulus, and apparent and complex moduli [90,91].

In conclusion, it should be emphasized that the presented results, and consequently the related discussions, are strongly affected by the specific constitutive parameters adopted in each hyperelastic model. Moreover, since numerous other hyperelastic formulations have been proposed in the literature, extending the analysis of generalized moduli to these models would provide a broader understanding of their mechanical behavior. In this context, the proposed methodology is fully

general and can be readily applied to different materials and their corresponding constitutive formulation and parameters.

## Funding

This research was partially funded by University of Padova - Department of Industrial Engineering, Project n° BIRD235152, titled "ERRA - Elastomeric scaffolds for soft tissue Repair, Replacement and Augmentation" and by Regione Veneto (Italy) PR Veneto FESR 2021–2027, project D19J24000820007 "RELIABLE - potere abilitante, comfort e sicurezza: strumenti per la sostenibilità e la fruibilità dei dispositivi per il lavoro, la moda e lo sport".

## CRediT authorship contribution statement

**Emanuele Luigi Carniel:** Writing – review & editing, Writing – original draft, Validation, Methodology, Investigation, Funding acquisition, Conceptualization.

## Declaration of competing interest

The authors declare the following financial interests/personal relationships which may be considered as potential competing interests:

Emanuele Luigi Carniel reports financial support was provided by University of Padova - Department of Industrial Engineering. Emanuele Luigi Carniel reports financial support was provided by Regione Veneto (Italy) PR Veneto FESR 2021–2027. If there are other authors, they declare that they have no known competing financial interests or personal relationships that could have appeared to influence the work reported in this paper.

## Appendix A

Regarding the different hyperelastic formulations, derivatives of the strain energy function can be computed as reported in Table A.1.

**Table A.1**
Analytical expressions of the first and second derivatives of the strain energy functions for the investigated isotropic hyperelastic formulations.

| | | |
|---|---|---|
| Neo-Hookean formulation | $W^{NH}(J,\widetilde{I}_1) = (K/2)(J-1)^2 + C_1(\widetilde{I}_1 - 3)$ | |
| $W^{NH}{}_1 = C_1 J^{-2/3}$ | $W^{NH}{}_2 = 0$ | $W^{NH}{}_J = K(J-1) - (2/3)C_1 J^{-5/3} I_1$ |
| $W^{NH}{}_{11} = 0$ | $W^{NH}{}_{22} = 0$ | $W^{NH}{}_{JJ} = K + (10/9)C_1 J^{-8/3} I_1$ |
| $W^{NH}{}_{12} = 0$ | $W^{NH}{}_{1J} = -(2/3)C_1 J^{-5/3}$ | $W^{NH}{}_{2J} = 0$ |
| **Mooney-Rivlin formulation** | $W^{MR}(J,\widetilde{I}_1,\widetilde{I}_2) = (K/2)(J-1)^2 + C_1(\widetilde{I}_1 - 3) + C_2(\widetilde{I}_2 - 3)$ | |
| $W^{MR}{}_1 = C_1 J^{-2/3}$ | $W^{MR}{}_2 = C_2 J^{-4/3}$ | $W^{MR}{}_J = K(J-1) - (2/3)C_1 J^{-5/3} I_1 - (4/3)C_2 J^{-7/3} I_2$ |
| $W^{MR}{}_{11} = 0$ | $W^{MR}{}_{22} = 0$ | $W^{MR}{}_{JJ} = K + (10/9)C_1 J^{-8/3} I_1 + (28/9)C_2 J^{-10/3} I_2$ |
| $W^{MR}{}_{12} = 0$ | $W^{MR}{}_{1J} = -(2/3)C_1 J^{-5/3}$ | $W^{MR}{}_{2J} = -(4/3)C_2 J^{-7/3}$ |
| **Fung-Demiray formulation** | $W^{FD}(J,\widetilde{I}_1) = (K/2)(J-1)^2 + (C_1/\alpha_1)\{\exp[\alpha_1(\widetilde{I}_1 - 3)] - 1\}$ | |
| $W^{FD}{}_1 = C_1 J^{-2/3}\exp\left[\alpha_1\left(J^{-2/3} I_1 - 3\right)\right]$ | $W^{FD}{}_2 = 0$ | $W^{FD}{}_J = K(J-1) - \frac{2}{3}C_1 J^{-5/3} I_1 \exp\left[\alpha_1\left(J^{-2/3} I_1 - 3\right)\right]$ |
| $W^{FD}{}_{11} = \alpha_1 C_1 J^{-4/3}\exp\left[\alpha_1\left(J^{-2/3} I_1 - 3\right)\right]$ | $W^{FD}{}_{22} = 0$ | $W^{FD}{}_{JJ} = K + (10/9)C_1 J^{-8/3} I_1 \exp\left[\alpha_1\left(J^{-2/3} I_1 - 3\right)\right] + (4/9)\alpha_1 C_1 J^{-10/3} {I_1}^2 \exp\left[\alpha_1\left(J^{-2/3} I_1 - 3\right)\right]$ |
| $W^{FD}{}_{12} = 0$ | $W^{FD}{}_{1J} = -(2/3)C_1 J^{-5/3}\left(1 + \alpha_1 J^{-2/3} I_1\right)\exp\left[\alpha_1\left(J^{-2/3} I_1 - 3\right)\right]$ | $W^{FD}{}_{2J} = 0$ |
| **Anssari-Benam formulation** | $W^{AB}(J,\widetilde{I}_1) = (K/2)(J-1)^2 + \frac{3(n-1)}{2n}\mu N\left[\frac{\widetilde{I}_1 - 3}{3N(n-1)} - \ln\left(\frac{\widetilde{I}_1 - 3N}{3 - 3N}\right)\right]$ | |
| $W^{AB}{}_1 = \frac{3(n-1)}{2n}\mu N\left[\frac{1}{3N(n-1)} - \frac{1}{J^{-2/3} I_1 - 3N}\right] J^{-2/3}$ | $W^{AB}{}_2 = 0$ | $W^{AB}{}_J = K(J-1) - \frac{(n-1)}{n}\mu N\left[\frac{1}{3N(n-1)} - \frac{1}{J^{-2/3} I_1 - 3N}\right] J^{-5/3} I_1$ |
| $W^{AB}{}_{11} = \frac{3(n-1)}{2n}\mu N \frac{J^{-4/3}}{\left(J^{-2/3} I_1 - 3N\right)^2}$ | $W^{AB}{}_{22} = 0$ | $W^{AB}{}_{JJ} = \frac{n-1}{n}\mu N\left\{\frac{2J^{-10/3} {I_1}^2}{3\left(J^{-2/3} I_1 - 3N\right)^2} + \frac{5}{3}\left[\frac{1}{3N(n-1)} - \frac{1}{J^{-2/3} I_1 - 3N}\right] J^{-8/3} I_1\right\}$ |
| $W^{AB}{}_{12} = 0$ | $W^{AB}{}_{1J} = -\frac{n-1}{n}\mu N\left\{\frac{J^{-7/3} I_1}{\left(J^{-2/3} I_1 - 3N\right)^2} + \left[\frac{1}{3N(n-1)} - \frac{1}{J^{-2/3} I_1 - 3N}\right] J^{-5/3}\right\}$ | $W^{AB}{}_{2J} = 0$ |

## Data availability

No data was used for the research described in the article.

## References

[1] Beda T. Modeling hyperelastic behavior of rubber: a novel invariant-based and a review of constitutive models. J Polym Sci B: Polym Phys 2007;45(13):1713–32. https://doi.org/10.1002/polb.20928.

[2] Dal H, Açıkgöz K, Badienia Y. On the performance of isotropic hyperelastic constitutive models for rubber-like materials: a state of the art review. Appl Mech Rev 2021;73(2):020802. https://doi.org/10.1115/1.4050978.

[3] Khaniki HB, Ghayesh MH, Chin R, Amabili M. Hyperelastic structures: a review on the mechanics and biomechanics. Int J Non Linear Mech 2023;148:104275. https://doi.org/10.1016/j.ijnonlinmec.2022.104275.

[4] Ricker A, Wriggers P. Systematic fitting and comparison of hyperelastic continuum models for elastomers. Arch Comput Methods Eng 2023;30:2257–88. https://doi.org/10.1007/s11831-022-09865-x.

[5] Carniel EL, Toniolo I, Fontanella CG. Computational biomechanics: in-silico tools for the investigation of surgical procedures and devices. Bioengineering 2020;7(2):48. https://doi.org/10.3390/bioengineering7020048.

[6] Martins PALS, Natal Jorge RM, Ferreira AJM. A comparative study of several material models for prediction of hyperelastic properties: application to silicone-rubber and soft tissues. Strain 2006;42(3):135–47. https://doi.org/10.1111/j.1475-1305.2006.00257.x.

[7] Motiwale S, Sacks MS. Structural constitutive models for soft biological tissues and biomaterials: the role of mechanical interactions. Mech Soft Mater 2025;7(1):1. https://doi.org/10.1007/s42558-024-00064-1.

[8] Lin PS, Le Roux de Bretagne O, Grasso M, Brighton J, StLeger-Harris C, Carless O. Comparative analysis of various hyperelastic models and element types for finite element analysis. Designs 2023;7:135. https://doi.org/10.3390/designs7060135.

[9] Amirreza A, Laksari K. Optimal experimental design for repeatable hyperelastic material characterization. J Mech Behav Biomed Mater 2025;170:107104. https://doi.org/10.1016/j.jmbbm.2025.107104.

[10] Natali AN, Carniel EL, Pavan PG, Dario P, Izzo I. Hyperelastic models for the analysis of soft tissue mechanics: definition of constitutive parameters. In: The First IEEE/RAS-EMBS International Conference on Biomedical Robotics and Biomechatronics, BioRob 2006. IEEE; 2006. p. 188–91.

[11] Zanelli L, Montanaro A, Carniel EL, Pavan PG, Natali AN. The study of equivalent material parameters in a hyperelastic model. Int J Non Linear Mech 2017;89:142–50. https://doi.org/10.1016/j.ijnonlinmec.2016.12.014.

[12] Gu L, Chafi MS, Ganpule S, Chandra N. The influence of heterogeneous meninges on the brain mechanics under primary blast loading. Compos B: Eng 2012;43(8):3160–6. https://doi.org/10.1016/j.compositesb.2012.04.014.

[13] Kochmann DM, Venturini GN. Homogenized mechanical properties of auxetic composite materials in finite-strain elasticity. Smart Mater Struct 2013;22:084004. https://doi.org/10.1088/0964-1726/22/8/084004.

[14] Perepelyuk M, Chin L, Cao X, van Oosten A, Shenoy VB, Janmey PA, Wells RG. Normal and fibrotic rat livers demonstrate shear strain softening and compression stiffening: a model for soft tissue mechanics. PLoS ONE 2016;11(1):e0146588. https://doi.org/10.1371/journal.pone.0146588.

[15] Fodor B, Kossa A. Stability study of the compressible Mooney-Rivlin hyperelastic model. J Strain Anal Eng Des 2024;59:258–68. https://doi.org/10.1177/03093247241233712.

[16] Kossa A, Valentine MT, McMeeking RM. Analysis of the compressible, isotropic, neo-Hookean hyperelastic model. Meccanica 2023;58:217–32. https://doi.org/10.1007/s11012-022-01633-2.

[17] Natali AN, Carniel EL, Gregersen H. Biomechanical behaviour of oesophageal tissues: material and structural configuration, experimental data and constitutive analysis. Med Eng Phys 2009;31(9):1056–62. https://doi.org/10.1016/j.medengphy.2009.07.003. 10.1109/BIOROB.2006.1639082.

[18] Toniolo I, Fontanella CG, Foletto M, Carniel EL. Coupled experimental and computational approach to stomach biomechanics: towards a validated characterization of gastric tissues mechanical properties. J Mech Behav Biomed Mater 2022;125:104914. https://doi.org/10.1016/j.jmbbm.2021.104914.

[19] Beatty MF, Stalnaker DO. The poisson function of finite elasticity. ASME J Appl Mech Dec 1986;53(4):807–13. https://doi.org/10.1115/1.3171862.

[20] Carniel EL, Berardo A, Toniolo I, Fontanella CG. Incremental moduli of isotropic hyperelasticity and parameters identification: polynomial, exponential and power law formulations. Int J Solids Struct 2025;321:113552. https://doi.org/10.1016/j.ijsolstr.2025.113552.

[21] Mihai LA, Goriely A. How to characterize a nonlinear elastic material? A review on nonlinear constitutive parameters in isotropic finite elasticity. Proc R Soc A 2017;473:20170607. https://doi.org/10.1098/rspa.2017.0607.

[22] Scott N. The incremental bulk modulus, Young's modulus and Poisson's ratio in nonlinear isotropic elasticity: physically reasonable response. Math Mech Solids 2007;12:526–42. https://doi.org/10.1177/1081286506064719.

[23] Biot MA. Incremental elastic coefficients of an isotropic medium in finite strain. Appl sci Res 1963;12:151–67. https://doi.org/10.1007/BF03184637.

[24] Carniel EL. Generalized incremental moduli of hyperelastic materials. ASME J Appl Mech 2025. https://doi.org/10.1115/1.4069072.

[25] Mahnken R, Dammann C. Simulation of strain-induced anisotropy for polymers with weighting functions. Arch appl mech 2014;84(1):21–41. https://doi.org/10.1007/s00419-013-0780-3.

[26] Flory P. Thermodynamic relations for high elastic materials. Trans Faraday Soc 1961;57:829–38. https://doi.org/10.1039/TF9615700829.

[27] Ogden RW. On the anisotropy of compressibility of rubber-like solids. J Phys D Appl Phys 1979;12(3):465. https://doi.org/10.1088/0022-3727/12/3/017.

[28] Hamed GR, Song JH. Anisotropy induced in an uncrosslinked elastomer via large strain deformation. Rubber Chem Technol 1985;58(2):407–20. https://doi.org/10.5254/1.3536074.

[29] Toki S, Sics I, Ran S, Liu L, Hsiao B. Molecular orientation and structural development in vulcanized polyisoprene rubbers during uniaxial deformation by in situ synchrotron X-ray diffraction. Polym (Guildf) 2003;44:6003–11. https://doi.org/10.1016/S0032-3861(03)00548-2.

[30] Horgan CO, Ogden RW, Saccomandi G. A theory of stress softening of elastomers based on finite chain extensibility. Proc R Soc Lond A: Math Phys Eng Sci 2004;460(2046):1737–54. https://doi.org/10.1098/rspa.2003.1248.

[31] Diani J, Brieu M, Vacherand JM. A damage directional constitutive model for Mullins effect with permanent set and induced anisotropy. Eur J Mech-A/Solids 2006;25(3):483–96.

[32] Dargazany R, Itskov M. A network evolution model for the anisotropic Mullins effect in carbon black filled rubbers. Int J Solids Struct 2009;46(16):2967–77. https://doi.org/10.1016/j.ijsolstr.2009.03.022.

[33] Machado G, Chagnon G, Favier D. Theory and identification of a constitutive model of induced anisotropy by the Mullins effect. J Mech Phys Solids 2014;63:29–39. https://doi.org/10.1016/j.jmps.2013.10.008.

[34] Marckmann G, Chagnon G, Le Saux M, Charrier P. Experimental investigation and theoretical modelling of induced anisotropy during stress-softening of rubber. Int J Solids Struct 2016;97:554–65. https://doi.org/10.1016/j.ijsolstr.2016.06.028.

[35] Anssari-Benam A, Akbari R, Dargazany R. Extending the theory of pseudo-elasticity to capture the permanent set and the induced anisotropy in the Mullins effect. Int J Non Linear Mech 2023;156:104500. https://doi.org/10.1016/j.ijnonlinmec.2023.104500.

[36] Vader D, Kabla A, Weitz D, Mahadevan L. Strain-induced alignment in collagen gels. PLoS ONE 2009;4(6):e5902. https://doi.org/10.1371/journal.pone.0005902.

[37] Ustinov KB. On induced anisotropy of mechanical properties of elastomers. Mech Solids 2019;54:1016–23. https://doi.org/10.3103/S0025654419070021.

[38] Mokhireva KA, Svistkov A, Shadrin V. Formation of anisotropic properties in elastomeric nanocomposites. Procedia Struct Integr 2021;32:137–43. https://doi.org/10.1016/j.prostr.2021.09.020.

[39] Xian W, Zhan YS, Maiti A, Saab AP, Li Y. Filled elastomers: mechanistic and physics-driven modeling and applications as smart materials. Polym (Basel) 2024;16(10):1387. https://doi.org/10.3390/polym16101387.

[40] Mahjoubi H, Zaïri F, Vozniak I, Tourki Z, Zaïri F. Modeling strain-induced dual-phase transformation in semicrystalline polylactide. Mech Time-Depend Mater 2023;27(4):989–1005. https://doi.org/10.1007/s11043-022-09563-y.

[41] Gajo A, Bigoni D. A model for stress and plastic strain induced nonlinear, hyperelastic anisotropy in soils. Int J Numer Anal Methods Geomech 2008;32(7):833–61. https://doi.org/10.1002/nag.648.

[42] Gajo A. Hyperelastic modelling of small-strain stiffness anisotropy of cyclically loaded sand. Int J Numer Anal Methods Geomech 2010;34(2):111–34. https://doi.org/10.1002/nag.793.

[43] Cudny M, Staszewska K. A hyperelastic model for soils with stress-induced and inherent anisotropy. Acta Geotech 2021;16:1983–2001. https://doi.org/10.1007/s11440-021-01159-z.

[44] Cudny M, Lisewska K, Winkler M, Marcher T. Modelling tunnelling-induced deformation in stiff soils with a hyperelastic-plastic anisotropic model. Acta Geotech 2024;19:4873–94. https://doi.org/10.1007/s11440-023-02202-x. 10.1016/j.euromechsol.2005.09.011.

[45] Manan N, Noor S, Azmi N, Mahmud J. Numerical investigation of ogden and mooney-rivlin material parameters. ARPN J Eng Appl Sci 2015;10:6329–35.

[46] Demiray H. A note on the elasticity of soft biological tissues. J Biomech 1972;5:309–11. https://doi.org/10.1016/0021-9290(72)90047-4.

[47] Fung YC. Elasticity of soft tissues in simple elongation. Am J Physiol 1967;213:1532–44. https://doi.org/10.1152/ajplegacy.1967.213.6.1532.

[48] Natali AN, Fontanella CG, Carniel EL. Constitutive formulation and numerical analysis of the heel pad region. Comput Methods Biomech Biomed Engin 2011;15:401–9. https://doi.org/10.1080/10255842.2010.539561.

[49] Carniel EL, Gramigna V, Fontanella CG, Stefanini C, Natali AN. Constitutive formulations for the mechanical investigation of colonic tissues. J biomed mater res A 2014;102(5):1243–54. https://doi.org/10.1002/jbm.a.34787.

[50] Anssari-Benam A. Large isotropic elastic deformations: on a comprehensive model to correlate the theory and experiments for incompressible rubber-like materials. J Elast 2023;153:219–44. https://doi.org/10.1007/s10659-022-09982-5.

[51] Gurtin ME. An introduction to continuum mechanics. Academic Press; 1981.

[52] Melly SK, Liu L, Liu Y, Leng J. A review on material models for isotropic hyperelasticity. Int J Mech Syst Dyn 2021;1:71–88. https://doi.org/10.1002/msd2.12013.

[53] Anssari-Benam A, Horgan CO. New constitutive models for the finite deformation of isotropic compressible elastomers. Mech Mater 2022;172:104403. https://doi.org/10.1016/j.mechmat.2022.104403.

[54] Itskov M. On the theory of fourth-order tensors and their application in computational mechanics. Comput Methods Appl Mech Eng 2000;189:419–38. https://doi.org/10.1016/S0045-7825(99)00472-7.

[55] Kellermann DC, Attard MM, O'Shea DJ. Fourth-order tensor algebraic operations and matrix representation in continuum mechanics. Arch Appl Mech 2021;91:4631–68. https://doi.org/10.1007/s00419-021-01926-0.

[56] Moakher M. Fourth-order cartesian tensors: old and new facts, notions and applications. Q J Mech Appl Math 2008;61(2):181–203. https://doi.org/10.1093/qjmam/hbm027.

[57] Itskov M. The derivative with respect to a tensor: some theoretical aspects and applications. ZAMM - J Appl Math Mech 2002;82:535–44. https://doi.org/10.1002/1521-4001(200208)82. :8<535::AID−AMM535>3.0.CO;2-U.

[58] Kintzel O, Başar Y. Fourth-order tensors - tensor differentiation with applications to continuum mechanics. Part I: classical tensor analysis. ZAMM 2006;86:291–311. https://doi.org/10.1002/zamm.200410242.

[59] Park SJ. Comparative study on hyperelastic constitutive models for the static and dynamic behavior of resilient mounts. Mater 2025;18:311. https://doi.org/10.3390/ma18020311.

[60] Yang P, Lei P, Liu B, Gao H. Construction of isotropic compressible hyperelastic constitutive models based solely on uniaxial tests. J Mech Phys Solids 2025;200:106150. https://doi.org/10.1016/j.jmps.2025.106150.

[61] Doll S, Schweizerhof K. On the development of volumetric strain energy functions. ASME J Appl Mech 2000;67(1):17–21. https://doi.org/10.1115/1.321146.

[62] Anssari-Benam A, Horgan CO. A three-parameter structurally motivated robust constitutive model for isotropic incompressible unfilled and filled rubber-like materials. Eur J Mech Solids 2022;95:104605. https://doi.org/10.1016/j.euromechsol.2022.104605.

[63] Anssari-Benam A, Horgan CO. On modelling simple shear for isotropic incompressible rubber-like materials. J Elast 2021;147:83–111. https://doi.org/10.1007/s10659-021-09869-x.

[64] Puglisi G, Saccomandi G. Multi-scale modelling of rubber-like materials and soft tissues: an appraisal. Proc R Soc A 2016;472:20160060. https://doi.org/10.1098/rspa.2016.0060.
[65] Destrade M, Ogden RW. On the third-and fourth-order constants of incompressible isotropic elasticity. J Acoust Soc Am 2010;128(6):3334–43. https://doi.org/10.1121/1.3505102.
[66] Niroomandi S, Alfaro I, Cueto E, Chinesta F. Model order reduction for hyperelastic materials. Int J Numer Methods Eng 2010;81(9):1180–206. https://doi.org/10.1002/nme.2733.
[67] Talebi S, Darijani H. A pseudo-strain energy density function for mechanical behavior modeling of visco-hyperelastic materials. Int J Mech Sci 2021;208:106652. https://doi.org/10.1016/j.ijmecsci.2021.106652.
[68] Agostiniani V, Dal Maso G, DeSimone A. Linear elasticity obtained from finite elasticity by Γ-convergence under weak coerciveness conditions. Annales de l'Institut Henri Poincaré C, Analyse non linéaire 2012;29(5):715–35. https://doi.org/10.1016/j.anihpc.2012.04.001.
[69] Green AE, Rivlin RS, Shield RT. General theory of small elastic deformations superposed on finite elastic deformations. Proc R Soc Lond A Math Phys Sci 1952;211(1104):128–54. https://doi.org/10.1098/rspa.1952.0030.
[70] Mott PH, Roland CM. Limits to Poisson's ratio in isotropic materials—General result for arbitrary deformation. Phys Scr 2013;87(5):055404. https://doi.org/10.1088/0031-8949/87/05/055404.
[71] Horgan CO, Murphy JG. Two different modes of shear stress response in simple shear of isotropic incompressible hyperelastic materials. J Elast 2023;154:81–90. https://doi.org/10.1007/s10659-022-09922-3.
[72] Moreira DC, Nunes LCS. Comparison of simple and pure shear for an incompressible isotropic hyperelastic material under large deformation. Polym Test 2013;32(2):240–8. https://doi.org/10.1016/j.polymertesting.2012.11.005.
[73] Destrade M, Murphy JG, Saccomandi G. Simple shear is not so simple. Int J Non Linear Mech 2012;47(2):210–4. https://doi.org/10.1016/j.ijnonlinmec.2011.05.008.
[74] Flory PJ. Network topology and the theory of rubber elasticity. Br polym j 1985;17(2):96–102. https://doi.org/10.1002/pi.4980170202.
[75] Song D, Oberai AA, Janmey PA. Hyperelastic continuum models for isotropic athermal fibrous networks. Interface Focus 2022;12(6):20220043. https://doi.org/10.1098/rsfs.2022.0043.
[76] Villani V, Lavallata V. The theories of rubber elasticity and the goodness of their constitutive stress–strain equations. Physchem 2024;4(3):296–318. https://doi.org/10.3390/physchem4030021.
[77] Treloar LRG. The physics of rubber elasticity. Oxford University Press; 1975.
[78] Wu PD, Van Der Giessen E. On improved network models for rubber elasticity and their applications to orientation hardening in glassy polymers. J Mech Phys Solids 1993;41(3):427–56. https://doi.org/10.1016/0022-5096(93)90043-F.
[79] Filho JCAD, Nunes LCS. Poisson function and volume ratio of soft anisotropic materials under large deformations. J Mech Behav Biomed Mater 2024;158:106689. https://doi.org/10.1016/j.jmbbm.2024.106689.
[80] Peel LD. Exploration of high and negative Poisson's ratio elastomer-matrix laminates. Phys stat sol (b) 2007;244:988–1003. https://doi.org/10.1002/pssb.200572717.
[81] Ting TCT. Very large Poisson's ratio with a bounded transverse strain in anisotropic elastic materials. J Elast 2004;77:163–76. https://doi.org/10.1007/s10659-005-2156-6.
[82] Guo Y, Qin Q, Han Z, Plamthottam R, Possinger M, Pei Q. Dielectric elastomer artificial muscle materials advancement and soft robotic applications. SmartMat 2023;4(4):e1203. https://doi.org/10.1002/smm2.1203.
[83] Micozzi F, Ragni L, Gioiella L, Quaglini V, Dall'Asta A. Variability of dynamic properties of rubber compounds for elastomeric bearings. Struct Control Health Monit 2023;2023(1):6638748. https://doi.org/10.1155/2023/6638748.
[84] Roeder CW, Stanton JF. Elastomeric bearings: state-of-the-art. J Struct Eng 1983;109(12):2853–71. https://doi.org/10.1061/(ASCE)0733-9445(1983)109:12(2853.
[85] Xavier MS, Fleming AJ, Yong YK. Finite element modeling of soft fluidic actuators: overview and recent developments. Adv Intell Syst 2021;3(2):2000187. https://doi.org/10.1002/aisy.202000187.
[86] Zhang Q, Yu W, Zhao J, Meng C, Guo S. A review of the applications and challenges of dielectric elastomer actuators in soft robotics. Machines 2025;13(2):101. https://doi.org/10.3390/machines13020101.
[87] Sasaki, K., Iwashimizu, Y., Kobori, O. (1990) Strain-induced elastic anisotropy measured with ultrasonic waves. 10.1115/1.2897663.
[88] Anani Y, Alizadeh Y. Visco-hyperelastic constitutive law for modeling of foam's behavior. Mater Des 2011;32(5):2940–8. https://doi.org/10.1016/j.matdes.2010.11.010.
[89] Caro AS, Chrysochoos A, Iaquinta S, Chagnon G. Modeling of nonlinear viscoelasticity and stress softening in soft tissues. Eur J Mech-A/Solids 2026;115:105818. https://doi.org/10.1016/j.euromechsol.2025.105818.
[90] Carniel EL. Analytical characterization of viscoelasticity in Zener and generalized Zener models under typical loading conditions. Mech Time-Depend Mater 2025;29:70. https://doi.org/10.1007/s11043-025-09810-y.
[91] Kossa A, Berezvai S. Visco-hyperelastic characterization of polymeric foam materials. Mater Today: Proc 2016;3(4):1003–8. https://doi.org/10.1016/j.matpr.2016.03.037.